Preprints of the 21st IFAC World Congress (Virtual)
Berlin, Germany, July 12-17, 2020

Model Identification of 2-DOF Lower Limb Exoskeleton with Neighborhood Field Optimization Algorithm ⋆

Zhenlei Chen * **Huiyu Xiong** ** **Xinran Wang** * **Qing Guo** *
Yan Shi *** **Yao Yan** * **Gan Liu** * **Dan Jiang** ****

* *School of Aeronautics and Astronautics, University of Electronic Science and Technology of China, and Aircraft Swarm Intelligent Sensing and Cooperative Control Key Laboratory of Sichuan Province, Chengdu, 611731, China, (e-mail: zhenlei_chen@std.uestc.edu.cn, wxr0104@163.com, guoqinguestc@uestc.edu.cn, y.yan@uestc.edu.cn, lg_uestc@163.com).*
** *Glasgow College, University of Electronic Science and Technology of China, Chengdu, 611731, China, (e-mail: 2017200506007@std.uestc.edu.cn)*
*** *School of Automation Science and Electrical Engineering, Beihang University, Beijing, 100191, China, (e-mail: shiyan@buaa.edu.cn)*
**** *School of Mechanical and Electrical Engineering, University of Electronic Science and Technology of China, Chengdu, 611731, China, (e-mail: jdan2002@uestc.edu.cn)*

Abstract: For the lower limb exoskeleton, the system control performance and stability of human-robot coordinated movement is often degraded by some model parametric uncertainties. To address this problem, the model parameter identification method based on Neighborhood Field Optimization (NFO) algorithm is proposed to obtain the accurate model parameters of 2-DOF exoskeleton, which guides the model-based controller design. For the 2-DOF lower limb exoskeleton experimental platform, the model is constructed by Lagrange equation. Meanwhile, the excitation trajectory with the setting mechanical constraints is designed by NFO to guarantee the identification accuracy. Meanwhile, the Huber fitness function is adopted to suppress the influence of the disturbance points in sampling dataset with respect to the identification accuracy. Finally, the NFO algorithm with the Huber fitness function is verified by 2-DOF lower limb exoskeleton experimental platform.

Keywords: Lower limb exoskeleton, Model identification, Excitation trajectory, Neighborhood Field Optimization, Huber fitness function.

1. INTRODUCTION

Recently, due to the aggravation of the population aging problem and the demand increase for patients undergoing rehabilitation training, the exoskeleton has became one of the research hot-point of medical rehabilitation. In order to ensure the motion safety, wearable comfort, and work efficiency of human-robot cooperative task, the exoskeleton has high requirements for response speed and stable performance. However, the traditional model-free controller is hard to achieve the desired requirements, while the model-based controller needs the precise system model. As a consequence, the efficient model parameters identification of exoskeleton is the prerequisite step of model-based controller design.

As introduced in the paper of Young and Ferris (2017), many contributions about model parameter identification of multi-link robot were proposed in some considerable literatures in recent years. For the system modeling, the exoskeleton dynamic model can be obtained by the Lagrange method or Newton-Euler method in Han et al. (2019) while the model parameter of the exoskeleton is hard to get by measuring.

Firstly, the excitation trajectory of data sampling experiment should be designed in advance to ensure the high quality of the sampling data and the dataset for a better identification in Swevers et al. (1997). For example, Bonnet et al. (2016) proposed the excitation trajectory design method for the legged system with mechanical constraints. Ayusawa et al. (2017) proposed the excitation trajectory design method based on the singular value of regressor matrices. Generally, the common methods for model parameter identification are the inverse dynamic identification model (IDIM) and least-squares estimation (LS) (Wu et al. (2010)), which are widely applied in various proto-

⋆ The corresponding author is Q. Guo. This work was supported by National Natural Science Foundation of China (No. 51775089 and 11872147), Sichuan Science and Technology Program (No. 2018JY0565, 20ZDYF3288).

Copyright lies with the authors

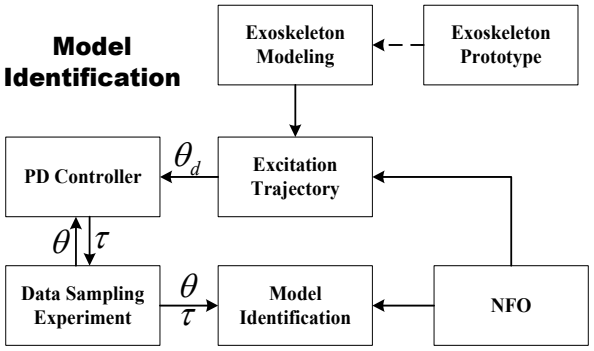

Fig. 1. Model identification structure

types and industrial robots (Gautier and Briot (2015)). In addition, with the development of Artificial Intelligence (AI) algorithms, many AI algorithms have been adopted in dynamic model identification of robotic, such as the artificial neural network in Yazdizadeh et al. (2000), the Particle Swarm Optimization (PSO) in He et al. (2017), etc. This paper is going to use an AI algorithm named Neighborhood Field Optimization (NFO) according to Wu (2013) which shows performance in terms of optimal accuracy and convergence speed.

Furthermore, for the the disturbance point introduced by data sampling error and poor filter designed, which degrades the model parameter identification accuracy, a popular function in M-estimation called Huber function (Huber et al. (1973)) employed as fitness function to address this problem for higher identification performance.

In summary, inspired by previous results on NFO (Wu (2013)) and the Huber fitness function (Huber et al. (1973)), the model identification method of 2-DOF lower limb exoskeleton is studied to accurately obtain the parameters of exoskeleton model. The main contribution of this paper are shown as follow:

(I) The NFO algorithm is not only adopted in the model parameter identification of exoskeleton but also design the excitation trajectory with motion constraints.

(II) The Huber fitness function is used to suppress the disturbance points of sampling dataset. In comparison with other common fitness function, the proposed Huber function has better identification accuracy and convergent velocity.

2. PROBLEM FORMULATION AND PRELIMINARIES

2.1 Identification Scheme of Identification

For the 2-DOF lower limb exoskeleton whose model parameters, such as element mass, moment of inertia, and centroid position, are difficult to be accurately measured, and the accurate dynamic model can be obtained by parameter identification with the high-quality method. The model identification structure is shown in Fig. 1.

2.2 Neighborhood Field Optimization

NFO algorithm is a class of group optimization algorithm, which is inspired by the interaction (gravity and repulsive)

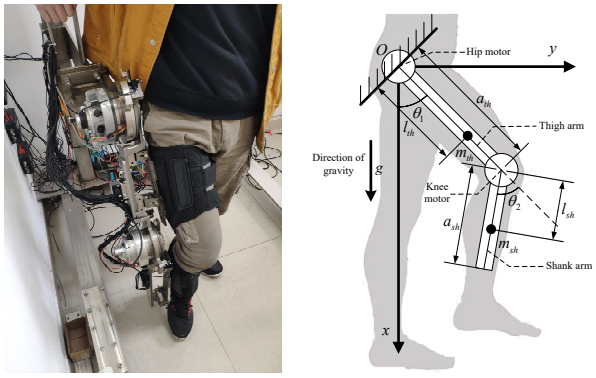

Fig. 2. Experimental prototype and mechanical structure

between natural particles and its neighborhood. Each particle in the group can move to a better place according to the NFO algorithm rule. Compared with the Genetic Algorithm(GA) and PSO, NFO has higher optimal accuracy and convergence speed since it effectively takes into account local information and global information.

For the D-dimension research space, randomize the initial N individuals. And for the i-th individual in the G-th generation $\mathbf{x}_{i,G} \in \mathbb{R}^D$, the the superior $\mathbf{xc}_{i,G} \in \mathbb{R}^D$ and inferior $\mathbf{xw}_{i,G} \in \mathbb{R}^D$ are defined as follows:

$$\begin{cases} \mathbf{xc}_{i,G} = \underset{f(\mathbf{x}_{k,G})<f(\mathbf{x}_{i,G})}{\arg\min} \|\mathbf{x}_{k,G} - \mathbf{x}_{i,G}\| \\ \mathbf{xw}_{i,G} = \underset{f(\mathbf{x}_{k,G})>f(\mathbf{x}_{i,G})}{\arg\min} \|\mathbf{x}_{k,G} - \mathbf{x}_{i,G}\| \end{cases}, \quad (1)$$

where $\mathbf{x}_{k,G}$ denotes the other individual, $f(\cdot)$ denotes the fitness function. Specially, $\mathbf{xc}_{i,G}$ is equivalent to $\mathbf{x}_{i,G}$ when $\mathbf{x}_{i,G}$ is the best individual in the population. Similarly, the worst individual $\mathbf{xw}_{i,G}$ is equivalent to $\mathbf{x}_{i,G}$. Then, defined the mutation factor as follow:

$$\begin{aligned} \mathbf{v}_{i,G} = \mathbf{x}_{i,G} &+ \alpha \cdot \mathbf{rand}(1) \cdot (\mathbf{xc}_{i,G} - \mathbf{x}_{i,G}) \\ &+ \alpha \cdot \mathbf{rand}(1) \cdot (\mathbf{xc}_{i,G} - \mathbf{xw}_{i,G}) \end{aligned}, \quad (2)$$

where α denotes the optimization rate which is the setting optimization parameter, $\mathbf{rand}(1) \in \mathbb{R}^D$ is random vector with each element belonging to $[0, 1]$. Subsequently, define the crossover vector as follow:

$$u_{j,i,G} = \begin{cases} v_{j,i,G}, & \text{if } \mathrm{rand}(0,1) \le Cr \text{ or } j = j_{\mathrm{rand}} \\ x_{j,i,G}, & \text{otherwise} \end{cases}, \quad (3)$$

where $j = 1, 2, \ldots, D$, $Cr = 0.5$ denotes the crossover factor, $\mathrm{rand}(0, 1)$ denotes a random number belong to $[0, 1]$ and j_{rand} is a random component to accept the new mutant vector. Finally, the better fitness between $\mathbf{u}_{i,G}$ and $\mathbf{x}_{i,G}$ is selected as the ith individual in the next generation.

3. MODELING AND IDENTIFICATION

3.1 Dynamic Model of Exoskeleton

Fig. 2 illustrates the mechanical structure diagram of the 2-DOF lower limb exoskeleton. The thigh arm and shank arm of the exoskeleton are securely connected with the operator's thigh and shank by force sensor respectively, and real-time human-robot interaction force can be accurately measured. Moreover, both hip and knee joint actuators of the exoskeleton are servo motor.

In the figure, the O, x, y respectively denote the origin, x-axis, y-axis of the inertial Cartesian coordinate, θ_1 and θ_2 respectively denote the hip and knee joint position, m_{th} and m_{sh} respectively denote the the thigh and shank weights, the a_{th} and a_{sh} respectively denote the thigh and shank length of exoskeleton, l_{th} denote the distance between the hip motor and centroid of exoskeleton thigh arm, l_{sh} denote the distance between the hip motor and centroid of exoskeleton shank arm. g denote gravity constant.

According to Siciliano et al. (2010), the dynamic model of 2-DOF lower limb exoskeleton is constructed by Lagrange technique as follow:

$$\mathbf{M}(\boldsymbol{\theta})\ddot{\boldsymbol{\theta}} + \mathbf{C}(\boldsymbol{\theta},\dot{\boldsymbol{\theta}})\dot{\boldsymbol{\theta}} + \mathbf{G}(\boldsymbol{\theta}) + \boldsymbol{\tau}_{\mathbf{f}}(\dot{\boldsymbol{\theta}}) = \boldsymbol{\tau} + \boldsymbol{\tau}_{\mathbf{dis}}, \quad (4)$$

where $\boldsymbol{\theta},\dot{\boldsymbol{\theta}},\ddot{\boldsymbol{\theta}} \in \mathbb{R}^2$ respectively denote the joint angle, joint angular velocity and joint angular acceleration of exoskeleton, $\boldsymbol{\tau} \in \mathbb{R}^2$ denotes the driving torque of servo motor, $\boldsymbol{\tau}_{\mathbf{f}}(\dot{\boldsymbol{\theta}})$ denotes the joint friction torque,$\boldsymbol{\tau}_{\mathbf{dis}} = \boldsymbol{J}^T(\boldsymbol{\theta})\mathbf{F}_{\mathbf{dis}}$ denotes the human-robot interaction torque where $\boldsymbol{J}^T(\boldsymbol{\theta}) \in \mathbb{R}^{2\times 2}$ is Jacobian matrix and $\mathbf{F}_{\mathbf{dis}}$ denote the human-robot interaction force. Furthermore, $\mathbf{M}(\boldsymbol{\theta})\ddot{\boldsymbol{\theta}} \in \mathbb{R}^{2\times 2}$, $\mathbf{C}(\boldsymbol{\theta},\dot{\boldsymbol{\theta}})\dot{\boldsymbol{\theta}}$ and $\mathbf{G}(\boldsymbol{\theta})$ denote inertia matrix, Coriolis matrix and gravity, and the detailed forms as follow

$$\mathbf{M}(\boldsymbol{\theta}) = \begin{bmatrix} M_{11} & M_{12} \\ M_{21} & M_{22} \end{bmatrix}, \mathbf{C}(\boldsymbol{\theta},\dot{\boldsymbol{\theta}}) = \begin{bmatrix} C_{11} & C_{12} \\ C_{21} & C_{22} \end{bmatrix}, \mathbf{G}(\boldsymbol{\theta}) = \begin{bmatrix} G_1 \\ G_2 \end{bmatrix}. \quad (5)$$

where $M_{11} = I_{th} + I_{sh} + m_{th}l_{th}^2 + m_{sh}a_{th}^2 + m_{sh}l_{sh}^2 + 2m_{sh}a_{th}l_{sh}\cos\theta_2$, $M_{12} = I_{sh} + m_{sh}l_{sh}^2 + m_{sh}a_{th}l_{sh}\cos\theta_2$, $M_{21} = I_{sh} + m_{sh}l_{sh}^2 + m_{sh}a_{th}l_{sh}\cos\theta_2$ and $M_{22} = I_{sh} + m_{sh}l_{sh}^2$. I_{sh} and I_{th} respectively denote the moment of inertia of exoskeleton shank and thigh arm. For the Coriolis matrix, $C_{11} = -2m_{sh}a_{th}l_{sh}\sin\theta_2\dot{\theta}_2$, $C_{12} = -m_{sh}a_{th}l_{sh}\sin\theta_2\ \dot{\theta}_2$, $C_{21} = m_{sh}a_{th}l_{sh}\sin\theta_2\dot{\theta}_1$ and $C_{22} = 0$. And $G_1 = l_{th}m_{th}g\sin\theta_1 + m_{sh}g(a_{th}\sin\theta_1 + l_{sh}\sin(\theta_1 + \theta_2))$ and $G_2 = l_{sh}m_{sh}g\sin(\theta_1+\theta_2)$. Additionally, $\boldsymbol{\tau}_{\mathbf{f}}(\dot{\boldsymbol{\theta}})$ denotes the joint friction torque, and the detailed form as follow:

$$\boldsymbol{\tau}_{\mathbf{f}}(\dot{\boldsymbol{\theta}}) = \begin{bmatrix} k_{1,1}\mathrm{sgn}(\dot{\theta}_1) + k_{1,2}\dot{\theta}_1 \\ k_{2,1}\mathrm{sgn}(\dot{\theta}_2) + k_{1,2}\dot{\theta}_2 \end{bmatrix}, \quad (6)$$

where $k_{i,1}, k_{i,2}(i = 1, 2)$ respectively denote the coulomb and viscous friction coefficient of hip and knee joint.

Lemma 1. The dynamic model of a multi-link system can be transformed into the minimum inertia linear form, hence (4) can be transformed into

$$\mathbf{M}(\boldsymbol{\theta})\ddot{\boldsymbol{\theta}} + \mathbf{C}(\boldsymbol{\theta},\dot{\boldsymbol{\theta}})\dot{\boldsymbol{\theta}} + \mathbf{G}(\boldsymbol{\theta}) + \boldsymbol{\tau}_{\mathbf{f}}(\dot{\boldsymbol{\theta}}) = \mathbf{Y}(\boldsymbol{\theta},\dot{\boldsymbol{\theta}},\ddot{\boldsymbol{\theta}})\boldsymbol{\Phi}, \quad (7)$$

where $\mathbf{Y} \in \mathbb{R}^{2\times 8}$ and $\boldsymbol{\Phi} \in \mathbb{R}^8$ denote the regression matrix and parameter vector, and the detailed forms as follow:

$$\Phi = \begin{bmatrix} \Phi^{(1)} & \Phi^{(2)} & \Phi^{(3)} & \Phi^{(4)} & \Phi^{(5)} & \Phi^{(6)} & \Phi^{(7)} & \Phi^{(8)} \end{bmatrix}^T, \quad (8)$$

where $\Phi^{(1)} = I_{th} + I_{sh} + m_{th}l_{th}^2 + m_{sh}a_{th}^2 + m_{sh}l_{sh}^2$, $\Phi^{(2)} = I_{sh} + m_{sh}l_{sh}^2$, $\Phi^{(3)} = m_{sh}a_{th}l_{sh}$, $\Phi^{(4)} = m_{th}a_{th}l_{th} - I_{th} - m_{th}l_{th}^2$, $\Phi^{(5)} = k_{1,1}$, $\Phi^{(6)} = k_{1,2}$, $\Phi^{(7)} = k_{2,1}$, $\Phi^{(8)} = k_{2,2}$, and all elements of Φ are constant parameter depending on the actual mechanical parameters of object. And

$$Y = \begin{bmatrix} Y^{(11)} & Y^{(12)} & Y^{(13)} & Y^{(14)} & Y^{(15)} & Y^{(16)} & Y^{(17)} & Y^{(18)} \\ Y^{(21)} & Y^{(22)} & Y^{(23)} & Y^{(24)} & Y^{(25)} & Y^{(26)} & Y^{(27)} & Y^{(28)} \end{bmatrix}, \quad (9)$$

where $Y^{(11)} = \ddot{\theta}_1 + e\sin\theta_1$, $Y^{(12)} = \ddot{\theta}_2 - e\sin\theta_1$, $Y^{(13)} = 2\cos\theta_2\ddot{\theta}_1 + \cos\theta_2\ddot{\theta}_2 - 2\sin\theta_2\dot{\theta}_1\dot{\theta}_2 - \sin\theta_2\dot{\theta}_2^2 + e\sin(\theta_1+\theta_2)$, $Y^{(14)} = e\sin\theta_1$, $Y^{(15)} = \mathrm{sgn}(\dot{\theta}_1)$, $Y^{(16)} = \dot{\theta}_1$, $Y^{(17)} = 0$, $Y^{(18)} = 0$, $Y^{(21)} = 0$, $Y^{(22)} = \ddot{\theta}_1 + \ddot{\theta}_1$, $Y^{(23)} = \cos\theta_2\ddot{\theta}_1 + \sin\theta_2\dot{\theta}_1^2 + e\sin(\theta_1+\theta_2)$, $Y^{(24)} = 0$, $Y^{(25)} = 0$, $Y^{(26)} = 0$, $Y^{(27)} = \mathrm{sgn}(\dot{\theta}_2)$, $Y^{(28)} = \dot{\theta}_2$ and $e = g/a_{th}$.

Because there is no human-robot interaction in the process of exoskeleton model identification, $\boldsymbol{\tau}_{\mathbf{dis}} = 0$ and the dynamic model as follow:

$$\boldsymbol{\tau} = \mathbf{Y}(\boldsymbol{\theta},\dot{\boldsymbol{\theta}},\ddot{\boldsymbol{\theta}})\boldsymbol{\Phi}. \quad (10)$$

The $\boldsymbol{\tau}$, $\boldsymbol{\theta}$, $\dot{\boldsymbol{\theta}}$ and $\ddot{\boldsymbol{\theta}}$ are obtained by real-time sampling, and Y is the known function. Consequently, if the all elements of Φ are identified accurately, the accurate dynamic model can be obtained.

For the N sets of sampling data, respectively define the sampling regression dataset $\bar{Y} \in \mathbb{R}^{2N\times 8}$ and sampling torque dataset $\bar{\tau} \in \mathbb{R}^2 N$ as follow:

$$\begin{aligned} \bar{Y} &= [Y^{(1)}, Y^{(2)}, \ldots, Y^{(n)}]^T \\ \bar{\tau} &= [\tau^{(1)}, \tau^{(2)}, \ldots, \tau^{(n)}]^T \end{aligned}, \quad (11)$$

where $\mathbf{Y}^{(i)}$ and $\boldsymbol{\tau}^{(i)}$ respectively denote regression matrix and torque vector based on i-th sampling data according to (9). According to the (10) and (11), define the current estimation parameter vector as $\hat{\boldsymbol{\Phi}}$ and current estimation torque $\hat{\boldsymbol{\tau}}$ as follow:

$$\hat{\boldsymbol{\tau}} = \bar{\mathbf{Y}}\hat{\boldsymbol{\Phi}}. \quad (12)$$

And the estimated torque error $\tilde{\boldsymbol{\tau}} = \bar{\boldsymbol{\tau}} - \hat{\boldsymbol{\tau}}$ is the important indicator of assessing $\hat{\boldsymbol{\Phi}}$.

3.2 Excitation Trajectory Design

Excitation trajectory is the desired trajectory of the data sampling experiment. Setting different excitation trajectory under the same sampling conditions may result in differences in some properties of the sampled data. For the exoskeleton model identification, And in the process of data sampling experiment, the external environmental disturbance and sensor sampling error may result in inaccurate sampling data and affect the accuracy of model parameter identification. To address this problem, a reasonable excitation trajectory can be designed to reduce the impact on the identification accuracy by the disturbance in the dataset.

Since Fourier series can theoretically approximate arbitrary waveform, the excitation trajectory is designed as follow:

$$\begin{aligned} \boldsymbol{\theta}_{\mathbf{d}} &= \boldsymbol{\theta}_{\boldsymbol{i},\mathbf{0}} + \sum_{k=0}^{N} \left(\mathbf{a}_{\mathbf{i},\mathbf{k}}\sin(k\omega_f t) + \mathbf{b}_{\mathbf{i},\mathbf{k}}\cos(k\omega_f t)\right) \\ \dot{\boldsymbol{\theta}}_{\mathbf{d}} &= \sum_{k=0}^{N} k\omega_f \left(\mathbf{a}_{\mathbf{i},\mathbf{k}}\cos(k\omega_f t) - \mathbf{b}_{\mathbf{i},\mathbf{k}}\sin(k\omega_f t)\right) \\ \ddot{\boldsymbol{\theta}}_{\mathbf{d}} &= \sum_{k=0}^{N} (k\omega_f)^2 \left(-\mathbf{a}_{\mathbf{i},\mathbf{k}}\sin(k\omega_f t) - \mathbf{b}_{\mathbf{i},\mathbf{k}}\cos(k\omega_f t)\right) \end{aligned}, \quad (13)$$

where $i = 1, 2$, $k = 1, \cdots, N$, $t \in [0, T]$ with the setting sampling period T, ω_f denotes the set fundamental frequency, k denotes the frequency coefficient, $\boldsymbol{\theta}_{\boldsymbol{i},\mathbf{0}}$ denotes the offsets of hip and knee joint excitation trajectory, $\mathbf{a}_{\mathbf{i},\mathbf{k}}$ and $\mathbf{b}_{\mathbf{i},\mathbf{k}}$ denote the parameter to be optimized, and the different values correspond to different trajectory.

For different identification objects, the constraints of the excitation trajectory design are set by analyzing the mechanical structure and the performance of related components. For the 2-DOF lower limb exoskeleton, by taking into account the limiter ensuring the safety and efficiency of the human-robot coordination system, the designed excitation trajectory has some motion constraints adapted for human walking gait listed in Table 1.

Table 1. Set motion constraints

Parameter	Restriction
Hip Angle θ_1	$[-0.13, 1.26]$(rad)
Hip Angular Velocity $\dot{\theta}_1$	$[-1.92, 1.92]$(rad/s)
Hip Angular Acceleration $\ddot{\theta}_1$	$[-5.16, 5.16]$(rad/s^2)
Knee Angle θ_2	$[-1.62, -0.23]$(rad)
Knee Angular Velocity $\dot{\theta}_2$	$[-1.64, 1.64]$(rad/s)
Knee Angular Acceleration $\ddot{\theta}_2$	$[-5.16, 5.16]$(rad/s^2)

In order to guarantee optimal efficiency and optimize performance, NFO is adopted in excitation trajectory design. According to (11), the current sampling regression dataset $\bar{\boldsymbol{Y}}$ can be calculated based on current excitation trajectory in ideal simulation environment. And compared with $\bar{\mathbf{Y}}^T\bar{\mathbf{Y}}$ and $\log\{\det\{\bar{\mathbf{Y}}^T\bar{\mathbf{Y}}\}\}$, the condition number of $\bar{\mathbf{Y}}$ is selected as the optimized criterion considering engineering practicality. Considering with the constraints in Table 1, the fitness function of NFO is shown as follow:

$$\mathrm{F}_{\mathrm{Tra}} = \begin{cases} \mathrm{Cond}(\bar{\mathbf{Y}}), & \text{if } \boldsymbol{\theta}, \dot{\boldsymbol{\theta}}, \ddot{\boldsymbol{\theta}} \in \text{Table 1} \\ \mathrm{Inf}, & \text{Otherwise} \end{cases}. \tag{14}$$

where $\mathrm{Cond}(\bar{\mathbf{Y}})$ represents the condition number of $\bar{\mathbf{Y}}$.

3.3 Exoskeleton Model Identification

Based on the excitation trajectory designed in last section, the sampling data can be obtained by data sampling experiment and dataset $\bar{\boldsymbol{Y}}$ and $\bar{\boldsymbol{\tau}}$ can be calculated according to (11). If the dataset are accurate enough, NFO is adopted in exoskeleton model identification to optimize $\hat{\Phi}$ making the estimated torque vector $\hat{\boldsymbol{\tau}} \to \bar{\boldsymbol{\tau}}$. Meanwhile, according to (10), the estimated parameter vector needs to be satisfied such that $\hat{\boldsymbol{\Phi}} \to \boldsymbol{\Phi}$. However, the corresponding model identification error $\tilde{\boldsymbol{\Phi}} = \hat{\boldsymbol{\Phi}} - \boldsymbol{\Phi}$ is unacceptable since lots of disturbance points are mixed in the dataset.

If the sampling data is accurate enough, the traditional sum of squared error(SSE) can be selected as the criterion of model identification to ensure the ideal identification accuracy. Hence, the fitness function can be set as follow:

$$\begin{aligned} \mathrm{F}_{\mathrm{SSE}} &= \sum_{i=0}^{N}\left(E^{(i)}\right), \\ E^{(i)} &= \tilde{\boldsymbol{\tau}}^{(i)T}\tilde{\boldsymbol{\tau}}^{(i)} \end{aligned} \tag{15}$$

where $E^{(i)}$ denotes the squared error of the i-th data. $\tilde{\boldsymbol{\tau}}^{(i)} = \hat{\boldsymbol{\Phi}}\bar{\mathbf{Y}}^{(i)} - \bar{\boldsymbol{\tau}}^{(i)}$ denotes the torque estimation error of the i-th data based on the current estimated parameter vector $\hat{\boldsymbol{\Phi}}$.

However, since the sampling noise is generated by the external environment disturbance and sensor noise, the disturbance point of sampling regression dataset $\bar{\boldsymbol{Y}}$ is generated by the first and second joint position derivatives

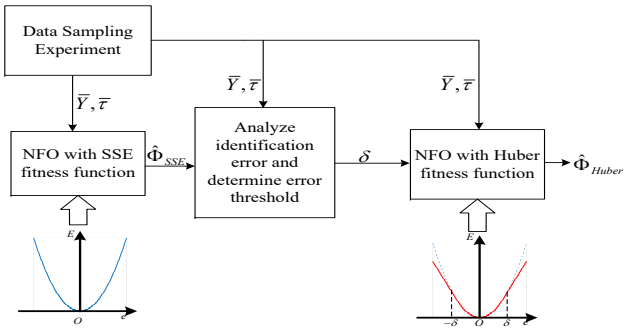

Fig. 3. Schematic diagram of identification process

$\dot{\boldsymbol{\theta}}$, $\ddot{\boldsymbol{\theta}}$. Meanwhile, for disturbance point of the sampling torque dataset $\bar{\boldsymbol{\tau}}$, since lots of chatters are mixed with the control torque signal because of the differentiator of PD controller in data sampling experiment, it is difficult to design the lowpass filter for sampling noise.

To address the above problem, inspired by the disturbance point processing in M-estimation (Huber et al. (1973)), design the fitness function of NFO with Huber function as follow:

$$\begin{aligned} \mathrm{F}_{\mathrm{Huber}} &= \sum_{i=0}^{N}\left(E^{(i)}\right) \\ E^{(i)} &= \begin{cases} \tilde{\boldsymbol{\tau}}^{(i)T}\tilde{\boldsymbol{\tau}}^{(i)}, & |\tilde{\boldsymbol{\tau}}^{(i)}| \le \boldsymbol{\delta}; \\ |\tilde{\tau}_1^{(i)}|^2 + 2\delta_2(|\tilde{\tau}_2^{(i)}| - \frac{\delta_2}{2}), & |\tilde{\tau}_1^{(i)}| \le \delta_1 \ |\tilde{\tau}_2^{(i)}| > \delta_2; \\ 2\delta_1(|\tilde{\tau}_1^{(i)}| - \frac{\delta_1}{2}) + |\tilde{\tau}_2^{(i)}|^2, & |\tilde{\tau}_1^{(i)}| > \delta_1 \ |\tilde{\tau}_2^{(i)}| \le \delta_2; \\ 2\boldsymbol{\delta}^T\left(|\tilde{\boldsymbol{\tau}}^{(i)}| - \frac{\boldsymbol{\delta}}{2}\right), & \text{Otherwise.} \end{cases} \end{aligned} \tag{16}$$

where $\tilde{\tau}_j^{(i)}(j = 1, 2)$ is the j-th element of $\tilde{\boldsymbol{\tau}}^{(i)}$, $\boldsymbol{\delta} = [\delta_1, \delta_2]^T$ is design torque error threshold.

According to (15), the value of torque error threshold $\boldsymbol{\delta}$ need to select from the relatively reasonable range. To address this problem, based on sampling dataset $\bar{\boldsymbol{Y}}$ and $\bar{\boldsymbol{\tau}}$, the initial identification result $\hat{\boldsymbol{\Phi}}_{\mathbf{SSE}}$ is gotten by NFO with SSE fitness function (15). Then, analysis the torque estimation error $\tilde{\boldsymbol{\tau}}$ based on $\hat{\boldsymbol{\Phi}}_{\mathbf{SSE}}$, and select 14% sampling point with bigger torque estimation error as disturbance point to select the value of $\boldsymbol{\delta}$. Finally, the identification result $\hat{\boldsymbol{\Phi}}_{\mathbf{Huber}}$ is obtained by NFO with Huber fitness function (16). The model parameter identification process of exoskeleton is shown in Fig. 3.

4. EXPERIMENT

In order to verify the theory and method in above, the experiment platform of 2-DOF lower limb exoskeleton has four functional parts as follows:

1) The signal acquisition module: the two joint positions, the human-robot interaction forces, and the driven torques are measured by the absolute encoders(INC-4-150 and INC-3-125), the 3-D force sensors (JNSH-2-10kg-BSQ-12)and torque sensor (integrating in the servo motor).

2) The control module: the control algorithm is programmed in Matlab/Simulink and compiled as a .os file,

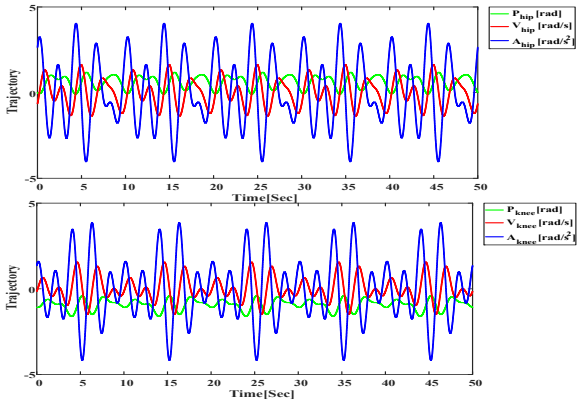

Fig. 4. Excitation trajectory of two joints

which is loaded into Labview and run in the system controller(cRIO-9035).

3) The execution module: the real-time control driven commands are executed by two servo motors(GDM1-100N2/120N2) and servo server driver(Elmo-G-SOLHR15/100E) to drive the 2-DOF lower limb exoskeleton prototype and to realize the desired motion.

Since the hip motor and knee motor need the different requirements for driving torque, the two different absolute encoders and servo motors are selected for different joints.

4.1 Excitation Trajectory Design

For the data sampling experiment, the NFO with fitness function (14) is used to design the excitation trajectory under the motion constraint shown in Table 1. And the individual number and iteration number of NFO respectively are set as 20 and 400, and $\boldsymbol{\theta_{i,0}} = [0.61\text{rad}; -0.925\text{rad}]$. Finally, the excitation trajectory parameters for for $\boldsymbol{\theta_d}$ in (13) is designed as a_{1hip}=0.99, b_{1hip}=1.28, a_{2hip}=-0.68, b_{2hip}=-9.73, a_{3hip}=-16.40, b_{3hip}=-15.52, a_{4hip}=11.49, b_{4hip}=-6.58, a_{5hip}=-11.03, b_{5hip}=-4.06, a_{1knee}=-4.53, b_{1knee}=7.80, a_{2knee} =3.53, b_{2knee}=-2.91, a_{3knee}=-0.73, b_{3knee}=-15.50, a_{4knee} =6.46, b_{4knee}=10.30, a_{5knee}=-7.94 and b_{5knee}=-8.75. Consequently, the excitation trajectories are shown in Fig. 4. And by analyzing Fig. 4, it can seen that $\boldsymbol{\theta_d}$ is restricted in the motion constraints.

4.2 Model Parameter Identification

Based on the dataset $\bar{\mathbf{Y}}$ and $\bar{\boldsymbol{\tau}}$ obtained by 35 sec duration of data sampling with $10ms$ sampling period, the 8 model parameters of both $\hat{\Phi}^{(i)}_{\mathbf{Huber}}(i = 1, \ldots, 8)$ and $\hat{\Phi}^{(i)}_{\mathbf{SSE}}(i = 1, \ldots, 8)$ are obtained by NFO with 40 individuals and 400 iterations. Firstly, the $\hat{\mathbf{\Phi}}_{\mathbf{SSE}}$ is obtained by NFO with SSE fitness function. Then, set the 14% of points, whose torque estimation error $\tilde{\boldsymbol{\tau}}$ is higher according to $\hat{\mathbf{\Phi}}_{\mathbf{SSE}}$,of dataset as disturbance point and the torque error threshold $\boldsymbol{\delta}$ is selected as $[138.46; 92.89]$. The parameters of $\hat{\mathbf{\Phi}}_{\mathbf{SSE}}$ are shown as $\hat{\Phi}^{(1)}_{SSE} = 27.97\text{kg} \cdot \text{m}^2$, $\hat{\Phi}^{(2)}_{SSE} = 12.15\text{kg} \cdot \text{m}^2$, $\hat{\Phi}^{(3)}_{SSE} = 1.79\text{kg} \cdot \text{m}^2$, $\hat{\Phi}^{(4)}_{SSE} = -8.41\text{kg} \cdot \text{m}^2$, $\hat{\Phi}^{(5)}_{SSE} = 31.83\text{kg}\cdot\text{m}$, $\hat{\Phi}^{(6)}_{SSE} = 15.25\text{N}\cdot\text{kg}\cdot\text{s}\cdot\text{rad}^{-1}$, $\hat{\Phi}^{(7)}_{SSE} = 52.39\text{kg}\cdot\text{m}$ and $\hat{\Phi}^{(8)}_{SSE} = -5.89\text{N} \cdot \text{kg} \cdot \text{s} \cdot \text{rad}^{-1}$. Meanwhile, the

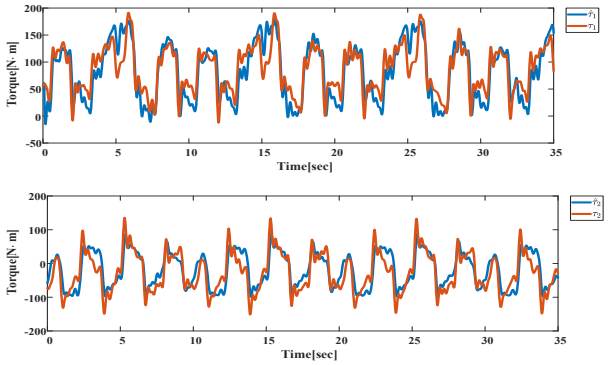

Fig. 5. The two estimated torques $\hat{\boldsymbol{\tau}}$ based on the identified parameter vector $\hat{\mathbf{\Phi}}_{\mathbf{SSE}}$ for $\boldsymbol{\theta_d}$

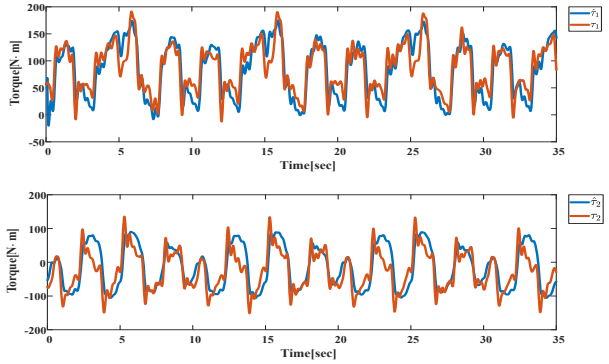

Fig. 6. The two estimated torques $\hat{\boldsymbol{\tau}}$ based on the identified parameter vector $\hat{\mathbf{\Phi}}_{\mathbf{Huber}}$ for $\boldsymbol{\theta_d}$

parameters of $\hat{\mathbf{\Phi}}_{\mathbf{Huber}}$ are shown as $\hat{\Phi}^{(1)}_{Huber} = 25.14\text{kg}\cdot\text{m}^2$, $\hat{\Phi}^{(2)}_{Huber} = 7.42\text{kg} \cdot \text{m}^2$, $\hat{\Phi}^{(3)}_{Huber} = 1.43\text{kg} \cdot \text{m}^2$, $\hat{\Phi}^{(4)}_{Huber} = -10.42\text{kg} \cdot \text{m}^2$, $\hat{\Phi}^{(5)}_{Huber} = 31.35\text{kg} \cdot \text{m}$, $\hat{\Phi}^{(6)}_{Huber} = 12.53\text{N} \cdot \text{kg} \cdot \text{s} \cdot \text{rad}^{-1}$, $\hat{\Phi}^{(7)}_{Huber} = 43.40\text{kg} \cdot \text{m}$ and $\hat{\Phi}^{(8)}_{Huber} = 28.01\text{N} \cdot \text{kg} \cdot \text{s} \cdot \text{rad}^{-1}$.

Based on the two identified parameter vectors $\hat{\mathbf{\Phi}}_{\mathbf{SSE}}$ and $\hat{\mathbf{\Phi}}_{\mathbf{Huber}}$, the two estimated torques $\hat{\boldsymbol{\tau}}$ are obtained and displayed in Fig. 5-6. It shows that two joint estimated values $\hat{\boldsymbol{\tau}}$ are consistent with the corresponding measured motor torques. The new verification trajectory $\boldsymbol{\theta_r}$ is randomly generated with the motion constraints to verify the reasonable parameter identification. Similarly, the estimated motor torque $\hat{\boldsymbol{\tau}}$ computed by two identified parameters $\hat{\mathbf{\Phi}}_{\mathbf{SSE}}$ and $\hat{\mathbf{\Phi}}_{\mathbf{Huber}}$ are shown in Figs. 7-8. In the verification experiment, the Huber performance of torque by using the identified parameters $\hat{\mathbf{\Phi}}_{\mathbf{Huber}}$ is better than that by using $\hat{\mathbf{\Phi}}_{\mathbf{SSE}}$ in the verification experiment and the SSE of $\hat{\boldsymbol{\tau}}$ based on the $\hat{\mathbf{\Phi}}_{\mathbf{Huber}}$ and $\hat{\mathbf{\Phi}}_{\mathbf{SSE}}$ is 6.53×10^9 and 1.03×10^{10}. Hence, the performance of estimated torque by using the identified parameter vector $\hat{\mathbf{\Phi}}_{\mathbf{Huber}}$ is better comparing with that by using $\hat{\mathbf{\Phi}}_{\mathbf{SSE}}$ in verification experiment.

4.3 NFO Performance Results

The NFO algorithm was used to design the excitation trajectory of data sampling experiment and identify the model parameters of 2-DOF lower limb exoskeleton. The

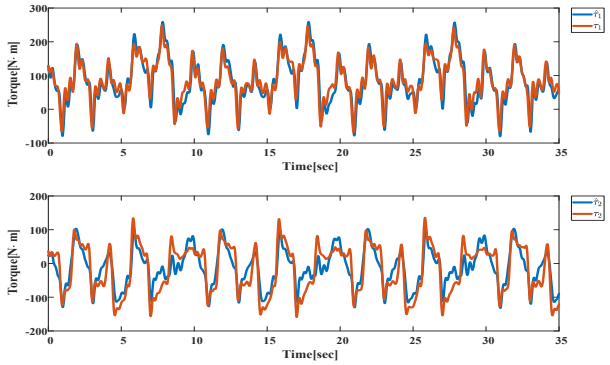

Fig. 7. The two estimated joint torques $\hat{\boldsymbol{\tau}}$ based on the identified parameter vector $\hat{\boldsymbol{\Phi}}_{\mathbf{SSE}}$ for $\boldsymbol{\theta}_{\mathbf{r}}$

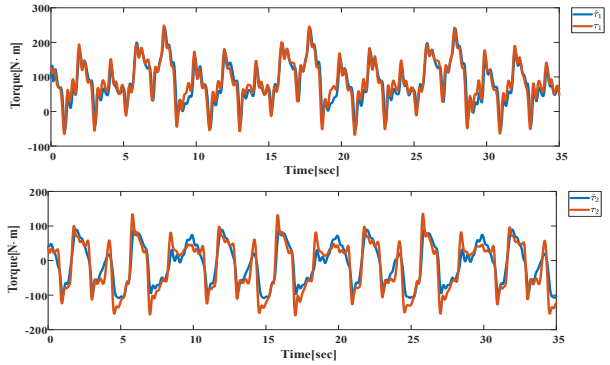

Fig. 8. The two estimated joint torques $\hat{\boldsymbol{\tau}}$ based on the identified parameter vector $\hat{\boldsymbol{\Phi}}_{\mathbf{Huber}}$ for $\boldsymbol{\theta}_{\mathbf{r}}$

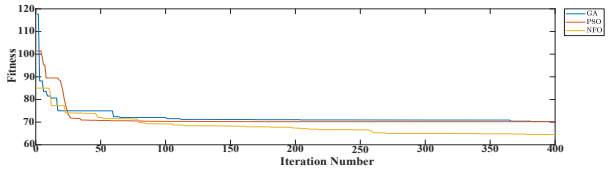

Fig. 9. Excitation trajectory optimization fitness curves

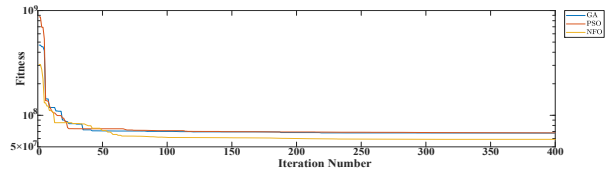

Fig. 10. Model parameter identification fitness curves with SSE

fitness optimization curves with respective to 3 optimization algorithm such as PSO, GA, NFO are shown in Fig. 9-10. Hence, it is clearly seen that the optimization accuracy and the optimization performance of NFO are better compared with PSO and GA.

5. CONCLUSION

In this study, the model parameter identification method of 2-DOF lower limb exoskeleton was proposed to ensure the identification accuracy and the convergence speed. Firstly, for the exoskeleton model, the excitation trajectory parameters was designed by NFO with fitness function (14) under restrictions in Table. 1. Then, the sampling dataset $\bar{\boldsymbol{Y}}$ and $\bar{\boldsymbol{\tau}}$ were obtained by the sampling data. Next, the NFO with Huber fitness function (16) was adopted to identify the model parameter vector, which improves the identification accuracy and show the better performance compared with SSE fitness function (15). Finally, the model identification method proposed above was verified by the identification experiment in 2-DOF lower limb exoskeleton experimental platform. The future works will identify online a modification of the model parameters, and compensate the influence on dynamic performance of model parameter variation.

REFERENCES

Ayusawa, K., Rioux, A., Yoshida, E., Venture, G., and Gautier, M. (2017). Generating persistently exciting trajectory based on condition number optimization. In *IEEE International Conference on Robotics & Automation*.

Bonnet, V., Fraisse, P., Crosnier, A., Gautier, M., and Venture, G. (2016). Optimal Exciting Dance for Identifying Inertial Parameters of an Anthropomorphic Structure. *IEEE Transactions on Robotics*, 32(4), 823–836.

Gautier, M. and Briot, S. (2015). Global Identification of Joint Drive Gains and Dynamic Parameters of Robots. *Multibody System Dynamics*, 33(1), 3–26.

Han, Y., Wu, J., Liu, C., and Xiong, Z. (2019). Static model analysis and identification for serial articulated manipulators. *Robotics and Computer-Integrated Manufacturing*, 57, 155–165.

He, W., Ge, W., Li, Y., Liu, Y.J., and Sun, C. (2017). Model Identification and Control Design for a Humanoid Robot. *IEEE Transactions on Systems Man & Cybernetics Systems*, 47(1), 45–57.

Huber, P.J. et al. (1973). Robust regression: asymptotics, conjectures and monte carlo. *The Annals of Statistics*, 1(5), 799–821.

Siciliano, B., Sciavicco, L., Villani, L., and Oriolo, G. (2010). *Robotics: modelling, planning and control*. Springer Science & Business Media.

Swevers, J., Ganseman, C., Tukel, D.B., De Schutter, J., and Van Brussel, H. (1997). Optimal robot excitation and identification. *IEEE transactions on robotics and automation*, 13(5), 730–740.

Wu, J., Wang, J., and Zheng, Y. (2010). An overview of dynamic parameter identification of robots. *Robotics & Computer Integrated Manufacturing*, 26(5), 414–419.

Wu, Z. (2013). Neighborhood field for cooperative optimization. *Soft Computing*, 17(5), 819–834.

Yazdizadeh, A., Khorasani, K., ., and Patel, R.V. (2000). Identification of a two-link flexible manipulator using adaptive time delay neural networks. *IEEE Transactions on Systems Man & Cybernetics Part B Cybernetics A Publication of the IEEE Systems Man & Cybernetics Society*, 30(1), 165–172.

Young, A.J. and Ferris, D.P. (2017). State of the Art and Future Directions for Lower Limb Robotic Exoskeletons. *IEEE Transactions on Neural Systems & Rehabilitation Engineering*, 25(2), 171–182.